Tuning the metal loading of Pt/CeO2 catalysts for the water-gas shift reaction

Clément Molinet-Chinaglia, Luis Alfonso Cardenas Arellano, Philippe Vernoux, Laurent Piccolo, Stéphane Loridant

Tuning the metal loading of Pt/CeO_2 catalysts for the water-gas shift reaction

Clément Molinet-Chinaglia, Luis Cardenas, Philippe Vernoux, Laurent Piccolo, Stéphane Loridant*

Université Claude Bernard-Lyon 1, CNRS, IRCELYON, UMR 5256, Villeurbanne, F-69100, France

** Corresponding author.*

E-mail address: stephane.loridant@ircelyon.univ-lyon1.fr

Abstract

The determination of active platinum species at the surface of Pt/CeO_2 catalysts is still a hot topic in the literature. In this work, an oxidizing pretreatment at 500 °C was applied to generate ultradispersed PtO_x species before the reaction. It is shown that the molar activity of such catalysts for the water gas shift reaction is strongly dependent on the platinum content, increasing by a factor of 2.5 from 0.1 to 0.6 wt% and stabilizing from 0.6 to 1.4 wt%. The tracking of Pt species present under reaction conditions (230 °C, $H_2O/CO=4$) was performed using *operando* DRIFT spectroscopy, CO-TPR and STEM in connection with the catalytic activity. A major structural change was found for Pt loadings above 0.6 wt% through the formation of metallic Pt^0 nanoparticles of ca 1.4 nm from oxidized Pt single atoms and clusters. Conversely, for Pt contents below 0.6 wt%, Pt species possess a stronger interaction with CeO_2 as well as a lower nuclearity, limiting their activation under reaction conditions. This strongly suggests that metallic Pt nanoparticles, prevalent at high loading, are more active than oxidic PtO_x single atoms and small clusters, which are predominantly present at low loading. This study highlights the key role of PtO_x reducibility and the importance to optimize the Pt loading to obtain active catalysts for the water-gas shift reaction.

Keywords: Pt/CeO_2 catalyst, water-gas shift reaction, oxidized Pt single atoms and clusters, metallic Pt nanoparticles, structural dynamics.

1. Introduction

The water-gas shift reaction (WGS, $CO + H_2O \leftrightarrow CO_2 + H_2$) is an essential step in different industrial processes employing hydrogen, such as the Haber-Bosch process and the methanol synthesis [1]. To face the difficulty of separating CO and H_2 without incurring significant economic and environmental costs, it was introduced to purify hydrogen and adjust its amount. This reaction is equilibrated and exothermic by about -41.1 $kJ.mol^{-1}$ under standard conditions, in the direction of H_2 and CO_2 formation [2]. Under industrial conditions, CO conversion is limited kinetically at low temperatures and thermodynamically at high temperatures, which has led to a major search for Low-Temperature Shift (LTS) catalysts [1].

The development of catalysts more active than the industrial ones at 190 – 250 °C is still a challenge [1]. Indeed, the use of industrial catalysts such as $Cu\text{-}ZnO\text{-}Al_2O_3$, leads to numerous issues due to a low activity requiring an increase in contact time, a CO partial order close to unity limiting the kinetics close to the equilibrium, a risk of ignition under exposure to air, and the need for pretreatments before each reaction run [1]. Many catalysts have been developed to find an alternative to the $Cu\text{-}ZnO\text{-}Al_2O_3$ reference. Among different systems, Pt/CeO_2 presents a high activity, selectivity, and stability for LTS [3–5].

A deep understanding of the reaction mechanism could lead to the development of Pt/CeO_2 catalysts with higher performance. To date, two mechanisms have been described in the literature, the redox and the associative ones, each involving adsorption of CO on a metallic atom and H_2O dissociation on an oxygen vacancy [6–8]. However, the identification of the different active species for the WGS reaction is still a matter of debate in the literature. For instance, it was shown that the support does not participate in the reaction [9] while the importance of the interface or oxygen vacancies was highlighted [10–12]. Moreover, some groups consider oxidized platinum atoms as active for the reaction [13–15], while others conclude that only the metallic ones are involved [16–22]. More precisely, Flytzani-Stephanopoulos and coworkers have concluded after leaching metallic nanoparticles (NPs) that cationic Pt species are the ones active for WGS [13,14]. Other studies have shown that ultradispersed oxidized species are little active in the reaction compared to metallic NPs [20,21]. Recent works indicate that the perimeter $Pt\text{-}O_v\text{-}Ce^{3+}$ sites of NPs are the most active for WGS, despite disagreement on the Pt oxidation state [16,22] and X. Li concluded that corner sites of small Pt clusters at the metal-support

interface are the dominant active sites, three orders of magnitude more active than other sites [20].

Investigating the influence of the metal loading on the catalyst activity by tracking Pt structural modifications is an interesting way to determine the role of platinum species in the reaction, as it has recently been shown by Maurer *et al.* for CO oxidation [23]. For WGS, different authors have previously studied the influence of the Pt content [14,15,24,25]. For example, Jacobs *et al*. have observed that the conversion increases with Pt content from 0 to 5 wt% after a reductive pretreatment under H_2 [25]. Nevertheless, most of these studies compare the influence of the loading by tracking the impact of the temperature at low temperatures of reaction (120 – 180 °C) or after reductive pretreatment, where structural modifications are not favored.

In this work, the impact of the Pt loading on the Pt/ceria catalyst state and performance has been studied between 0.1 and 1.7 wt% Pt. An oxidative pretreatment at 500 °C was applied because it allows to ultradispersed platinum atoms at the surface of CeO_2 before submitting the catalyst to highly reducing WGS conditions, which favor Pt agglomeration [26]. To explain the influence of metal loadings on dispersion, and redox modification of platinum species under reaction conditions, the catalysts were characterized by crossing different techniques. As a result, a relationship between the nature of Pt species present in the catalysts depending on the Pt loading and the catalytic activity was established.

2. Experimental

2.1. Catalyst preparation

Pt/CeO_2 catalysts with various loadings were prepared by wet impregnation of 2 g of CeO_2 (150 $m^2.g^{-1}$, Solvay Special Chem Company) with 24 mL of $Pt(NH_3)_4(NO_3)_2$ (>99% purity, Sigma Aldrich) precursor solution at 60 °C for 4 h under a stirring of 400 rpm. Water was then removed with a rotary evaporator at a temperature of 70 °C and a pressure of 200 mbar. The obtained powder was dried and finally calcined under air flow of 100 $NmL.min^{-1}$ at 500 °C (heating rate 10 °C. min^{-1}) during 4 h. The samples are labelled xPt with x corresponding to the Pt weight percent determined by X-ray Fluorescence (XRF).

2.2. Catalyst characterization

Pt loading quantification was carried out by X-ray Fluorescence (L_α band) by placing approximately 1 g of sample, previously ground, in a capsule under a He flow of a Malvern Panalytical Epsilon 4 spectrometer and using a calibration curve determined from ICP-OES measurements (Figure S1).

The S_{BET} surface areas of Pt/CeO_2 samples were determined with an ASAP 2020 (Micromeritics) apparatus by nitrogen physisorption volumetry at -196 °C after pretreatment at 300 °C under a vacuum of 10^{-3} mbar using a Smart Vac Prep (Micromeritics) apparatus.

The powder X-Ray Diffraction (XRD) analyses were carried out in a Bragg-Brentano optical configuration on a Bruker D8 Advance A25 equipped with a LynxEye XE-T detector. The K_α line of Cu (λ=1.54184 Å) was used as emission source. Diffractograms were recorded from 4 to 80 ° with a goniometer using a step size of 0.02 ° and an acquisition time of 0.5 s per step and processed using the Diffrac.eva software. Furthermore, the crystallite size was determined using the Scherrer equation: $D=K\lambda/(\beta i*\cos(\theta))$ where D is the crystallite size, λ the wavelength of the X-ray beam, βi the full width at half-maximum corrected of the instrumental width (0.06 °) and θ the diffraction peak angle. After reaction, diffractograms were also recorded between 37 and 40 ° with a step size of 0.02 ° and an acquisition time of 12 s per step.

A Titan ETEM G2 80-300 kV (FEI) microscope equipped with a spherical aberration corrector was operated at 300 kV for the Scanning Transmission Electron Microscopy (STEM) analyses, which were mainly carried out in Annular Dark Field (ADF) mode (resolution better than 0.136 nm) under ultrahigh vacuum. A few milligrams of the sample were ground and ultrasonically suspended in ethanol for each preparation. Two to three drops of the suspension were deposited on the surface of the holey carbon film covering a 300-mesh copper grid. Further analyses were carried out on a JEM-ARM200F Cold FEG microscope operated at 200 kV equipped with a Cs probe corrector and cold field emission source for the Scanning Transmission Electron Microscopy (STEM) analyses. The obtained resolution is 0.78 Å in High-Angle Annular Dark Field (HAADF) mode under ultrahigh vacuum with the GATAN detector. EDX analyses were performed using a CENTURIO-X SDD detector (129 eV resolution).

MicroRaman spectra were recorded in ambient air with a LabRAM HR (Horiba) spectrometer equipped with an Edge filter, a diffraction grating (300 line.mm^{-1}) and a CCD detector cooled at -75 °C. An x50 microscope objective was chosen to focus the laser light (514

nm, 0.3 mW) and recollect the backscattered light. The spectral and spatial resolutions were 4 cm^{-1} and 2 μm, respectively. The acquisition time was 40 s for the 100-2000 cm^{-1} spectral range.

Temperature-Programmed Reduction under CO (CO-TPR) curves were obtained using a 9 Omnistar GSD 301 O2 (Pfeiffer Vacuum) mass spectrometer coupled to a flow fixed bed reactor setup. For each gas, the flowrate was monitored by a Brooks flowmeter. A tubular furnace heated the reactor, with the use of one thermocouple in the furnace and another at the powder bed level. The sample (50 mg) was placed in a U-shape reactor (internal diameter of 4 mm) on a quartz fibber pad, pretreated under 40 $NmL.min^{-1}$ of 1%O_2/He to remove surface species at 500 °C during 1 h (OX1) and then exposed to 40 $NmL.min^{-1}$ of 1% CO/He while heating from room temperature (RT) to 500 °C (10 $°C.min^{-1}$) after stabilization of the CO signal (m/z = 28) and then waiting for 1 h at 500 °C. Both the signals at *m/z* = 28 and 44 were recorded to quantity the CO consumption and CO_2 production, respectively.

Diffuse Reflectance Infrared Fourier Transform (DRIFT) spectra were obtained with a Thermo Nicolet IR-TF 6700 spectrometer equipped with a ceramic source, a high sensitivity MCT detector cooled by liquid nitrogen and a Harrick-HVC-DRP cell for *in situ* and *operando* experiments. They were recorded with the Thermo OMNIC software, averaging 32 scans at a spectral resolution of 4 cm^{-1}. Prior to each CO chemisorption experiment, the catalysts were pretreated at 500 °C for 1 h under 20% O_2-He flow of 50 $NmL.min^{-1}$ for the fresh catalysts or under He for the spent ones. CO chemisorption was carried out from -10 to 20 °C on 50 mg of the catalyst under a 2% CO/He flow at 25 NmL/min. For CO-TPR monitored by DRIFT spectroscopy, the catalysts were pretreated under synthetic air at 500 °C. A temperature ramp of 10 °C/min under 25 NmL/min of 2% CO/He was then applied to the Harrick cell with steps at 50, 100, 145, 190, 234 and 279 °C for 30 min each. *Operando* measurements were carried out at 230 °C under P_{CO} = 5 mbar and P_{H2O} = 20 mbar (H_2O/CO ratio=4). The *GHSV* value was 1000 $mL.min^{-1}.g^{-1}$. Spectra were recorded every minute during the reaction. In both cases, the background corresponded to the spectra of KBr recorded at the same temperatures. An Inficon Transpector CPM 3 mass spectrometer was placed at the reactor outlet to analyze the gas composition.

High-resolution X-ray Photoelectron Spectroscopy (HR-XPS) measurements were carried out using a commercial KRATOS Ultra-DLD spectrometer equipped with a monochromatic Al

K_α source (1486.6 eV). The charge energy shift of the Pt 4f spectra was corrected by fixing the adventitious carbon C 1s core level at 284.6 eV. The Pt 4f fitting decomposition was performed using a combination of Voigt line shapes.

2.3. Catalytic measurements

For WGS tests, the catalysts were introduced in a straight Pyrex reactor with an internal diameter of 1 cm. The gas lines were separated into two parts: one for the reaction mixture and another one for the pretreatment since the reactor was fed by different gas lines: Ar and He as carrier and tracer gases, O_2 for pretreatment, H_2O and CO for the reaction. The gaseous H_2O flow was obtained using a KDS syringe pump equipped with a 25 mL Terumo syringe and a homemade vaporizer at 150 °C. The flow rates were controlled by Bronkhorst flowmeters for He/O_2 and Brooks ones for CO/Ar. The mixing of the gases was done in a heating box at a temperature of 150 °C to avoid water condensation while homogenizing the reaction mixture. The output analysis was performed using an Inficon Transpector CPM 3 mass spectrometer (MS) controlled with the FabGuard software. A catalyst mass of 200 mg sieved between 106 and 180 µm was placed in the reactor. Prior to any catalytic test, a treatment under 100 NmL/min of a 20% O_2/Ar mixture was carried out at 500 °C for 1 h. The flow rates were 40 $NmL.min^{-1}$ for H_2O, 10 NmL/min for CO and 65 NmL/min for Ar (H_2O/CO/Ar/He:33.3/8.3/54.2/4.2%). He (5 NmL/min) was used as an internal standard for MS analysis. Considering the catalyst mass and the total flow rate, the GHSV value was 600 $mL.min^{-1}.g^{-1}$.

The following equations were used to determine the Y_{H2} yield and the R molar activity:

$$Y_{H2}\ (\%) = \frac{C_{H2,out}}{C_{CO,out} + C_{H2,out}} \times 100$$

$$R(mol_{H2}.mol_{Pt}{}^{-1}.s^{-1}) = \frac{Y_{H2} \times F_{CO}}{n_{Pt}}$$

with $C_{X,out}$ the molar concentration (bar) of compound X at the outlet, F_{CO} the CO molar flow rate (mol/s). $C_{CO,out} + C_{H2,out}$ was used instead of $C_{CO,in}$ in the calculation of Y_{H2} to limit uncertainties of measurement due to water condensation in the trap after the reactor. It is valid as the selectivity to H_2 and CO_2 was ca. 100%. Preliminary measurements varying the mass of catalyst from 50 to 200 mg and its granulometry from 50-80 to 106-180 µm demonstrated the

absence of external and internal diffusion limitations for a large range of conversion. The granulometry was then fixed to 106-180 μm.

3. Results and discussion

3.1. Characterization of Pt/CeO_2 at the fresh state

The platinum content of the Pt/CeO_2 catalysts varied from 0.10 to 1.72 wt% (Table S1), as determined by XRF. Their S_{BET} specific surface areas were close to that of bare CeO_2 (152 $m^2.g^{-1}$), leading to a Pt surface content varying from 0.02 to 0.35 $Pt.nm^{-2}$, which is much lower than the theoretical monolayer value (15.2 $Pt.nm^{-2}$ for Pt(111)) [27].

The X-ray diffractograms of the fresh catalysts correspond to cubic CeO_2 (Figure 1) with a crystallite size of 7-8 nm. Additional peaks due to PtO_x and Pt^0 crystalline phases were not detected, suggesting a high platinum dispersion. Nevertheless, the main diffraction peak at 39.7° relative to the Pt(111) plane of Pt^0 was slightly above the noise level for the 1.72Pt catalyst (see the zoom in Figure 1). This suggests a potential redox process during the calcination step leading to the formation of Pt^0.

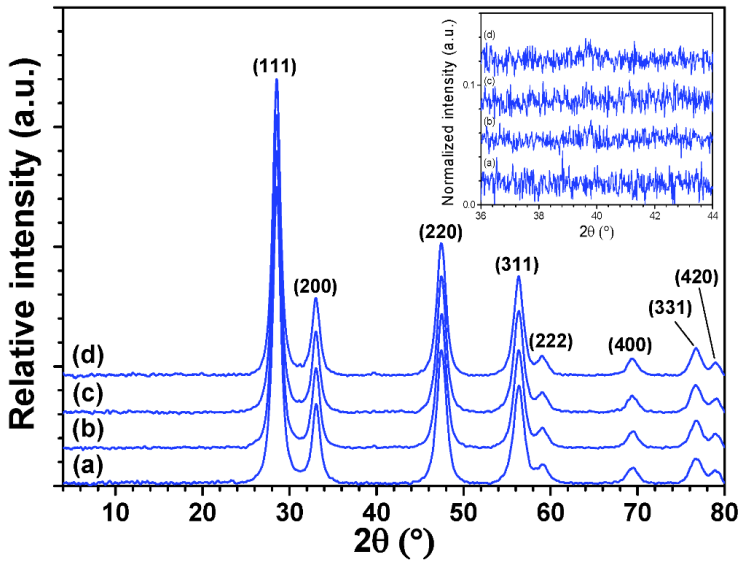

Figure 1. X-ray diffractograms of (a) 0.59Pt, (b) 0.80Pt, (c) 1.06Pt and (d) 1.72Pt catalysts in the fresh state between 10 and 80°, and zoomed between 36 and 44° (insert). The peaks are indexed with those of cubic CeO_2.

STEM-ADF images recorded with a Titan ETEM G2 microscope show CeO_2 crystallites (Figure S2) but do not reveal any platinum structure in the fresh catalysts, suggesting that Pt is in an ultradispersed state [26] in the form of subnanometric clusters and/or single atoms (SAs), as reported by Lin *et al.* and Ferré *et al*. after calcination [28,29]. Indeed, as the atomic numbers of

Pt and Ce are close (58 and 78, respectively), as CeO_2 crystallites are relatively thick (7-8 nm) and as the structure of PtO_x could be two-dimensional with a lower density of Pt than in metallic Pt^0, it is difficult to observe subnanometric PtO_x species on CeO_2 [30,31]. However, by using a JEM-ARM200F Cold FEG probe-corrected microscope, both Pt clusters and SAs were distinguished in the 1.72Pt catalyst (Figure 2). When recording the EDX spectrum coming from areas where such species were clearly identified or suspected, the M band at 2.048keV of Pt was observed (Figure S3). It was previously shown by XPS that these species mostly contain Pt^{2+} cations [29].

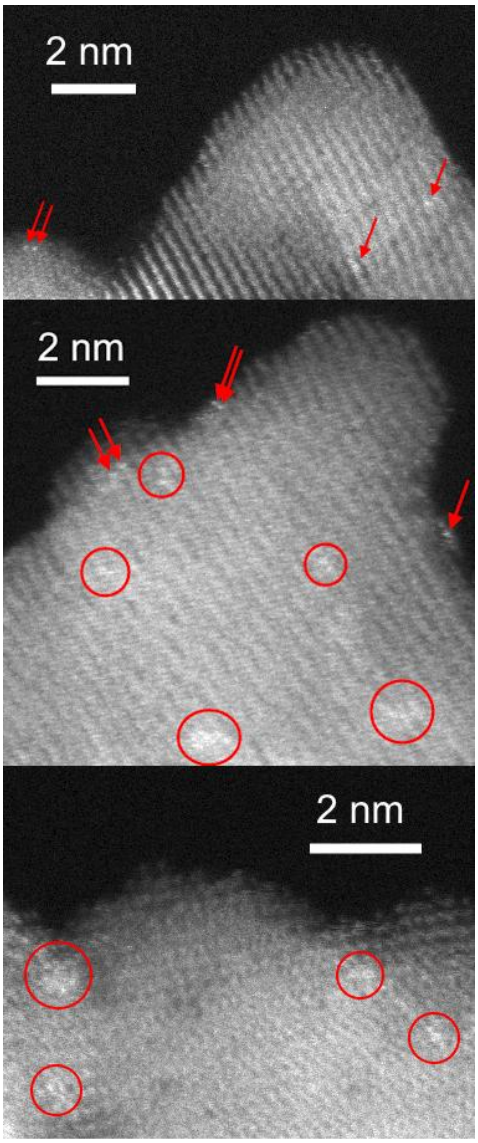

Figure 2. STEM-HAADF images recorded with a JEM-ARM200F Cold FEG corrected microscope of 1.72Pt catalyst in the fresh state. Red arrows point to Pt SAs while Pt clusters are circled.

Raman spectra of the Pt/CeO_2 catalysts (Figure 3a) show the characteristic bands of nanocrystalline CeO_2 with the F_{2g} band at 460 cm^{-1}, the surface modes of the (111) planes at 240 and 400 cm^{-1}, the defect D band near 595 cm^{-1} and the 2LO second-order band at 1165 cm^{-1} [32]. In addition, the bands near 560 and 660-685 cm^{-1} are attributed either to ν_{as}(Pt-O-Ce) and ν_s(Pt-O-Ce) stretching vibrations [33] or ν(Pt-O-Ce) and ν(Pt-O) stretching vibrations [28] of PtO_x species highly dispersed on the surface of CeO_2, respectively. The first attribution assumes that only Pt-O-Ce bridging bonds are observed by Raman spectroscopy while terminal Pt-O bonds would also be observed in the second assumption. For the sake of simplicity, the second band is labeled ν(PtO_x) in the following. Note that the two bands cannot be attributed to crystalline PtO, Pt_3O_4, α-PtO_2 or β-PtO_2 but are rather close to those of Pt_5O_6 (main bands at 509-527 and 642-670 cm^{-1}) [34].

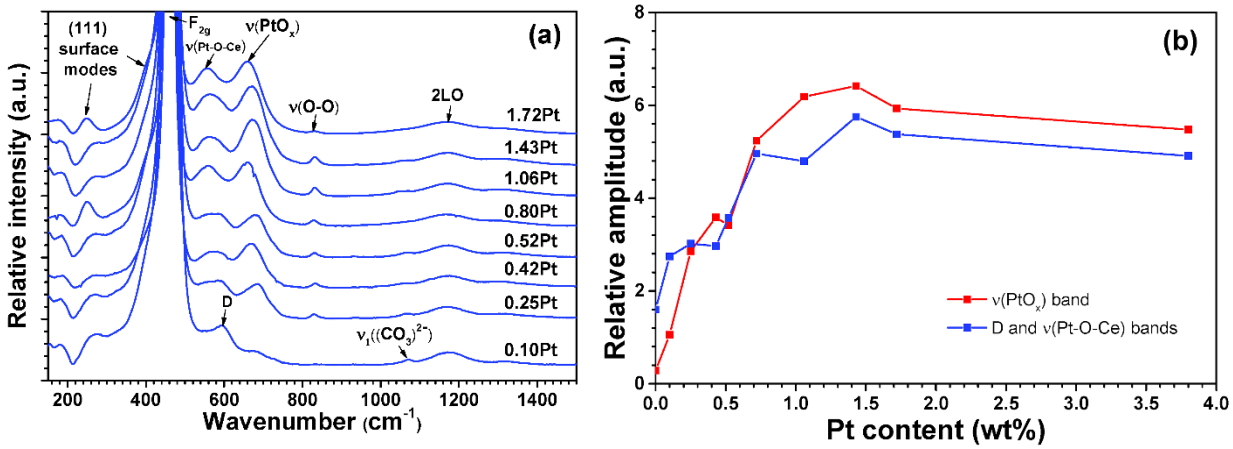

Figure 3. (a) Raman spectra of Pt/CeO_2 catalysts in the fresh state and (b) Relative amplitude of the ν(PtO_x) band around 670 cm^{-1} as a function of the Pt content after normalization to the amplitude of the 2LO band.

The relative amplitude of the ν(Pt-O-Ce) and ν(PtO_x) bands increases with the Pt content until reaching a plateau at around 0.80-1.06 wt% of Pt (Figure 3b). The amplitude of the former band is initially higher because of the D band contribution and possibly a high proportion of Pt-O-Ce bonds. The plateau observed for contents above 1.06 wt% suggests that other Pt species than PtO_x are present but they badly respond by Raman spectroscopy and are not detected.

CO-DRIFT spectra of Pt/CeO_2 catalysts recorded from -10 to 20 °C are plotted in Figure 4. The spectra recorded at -10 °C exhibit two bands at 2156 and 2173 cm^{-1} resulting from coulombic interaction between CO and Ce^{3+} as well as CO and Ce^{4+} Lewis acid sites, respectively [35]. Note that the strength of these sites is relatively weak considering the slight

shift of the two bands compared to the gas phase ($\nu(CO)_{gas}$=2143 cm^{-1}) [36]. Those bands disappear when increasing the temperature to 20 °C. No other significant band was observed for the 0.10Pt catalyst while the main band was located at 2090 cm^{-1} for 0.59Pt, 0.80Pt and 1.06Pt. It was attributed either to CO molecules adsorbed on oxidized Pt clusters [31,37,38] or on SAs [30,38–40] in the literature. According to Resasco et *al.* [31], the interaction between Pt SAs and CO is weak at room temperature limiting identification of such species. It arises from their saturated coordination shell leading to a low propensity to form additional bonds with CO (predicted CO adsorption energy of ~10 $kJ.mol^{-1}$).[31] Therefore, the spectrum of the 0.10Pt catalyst at 20 °C suggests that this catalyst only contains SAs. Note that the same authors assumed that above a content of 0.10 wt%, the sites stabilizing the Pt SAs on the surface of the used commercial ceria used become saturated.

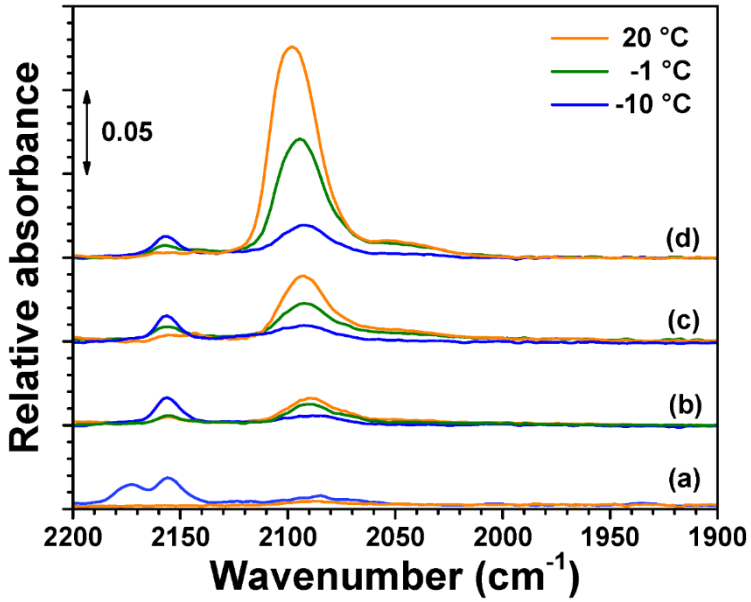

Figure 4. CO-DRIFT spectra between 1900 and 2200 cm^{-1} of the (a) 0.10Pt, (b) 0.59Pt, (c) 0.80Pt and (d) 1.06Pt catalysts recorded from -10 to 20 °C under 25 $NmL.min^{-1}$ of 2%CO/He. The backgrounds correspond to the spectra of pretreated samples recorded at the same temperatures and the $\nu(CO)_{gas}$ signal is subtracted.

Concerning the three other catalysts, the band at 2090 cm^{-1} is attributed to PtO_x clusters present in addition to SAs. For such species, significant undercoordination of Pt atoms to oxygen enables simultaneous strong CO binding [31]. However, the absorbance of this band increased with CO chemisorption temperature from -10 to 20 °C. This indicates a reactive process, leading to a higher proportion of clusters and potentially causing a misinterpretation of the spectral evolution as a function of Pt content. Note that bidentate carbonates (bands at 1575, 1294 and

1028 cm^{-1})[37–39] and hydrogen carbonates (bands at 1391 and 1217 cm^{-1})[37–39] were formed in parallel (Figure S4) suggesting that a redox mechanism occurred. As measurements at liquid nitrogen temperature are required to avoid this reactive process and as our experimental set-up did not allow it, this technique was not further used for fresh Pt/CeO_2 catalysts.

3.2. Impact of the Pt loading on the catalytic activity

Pt/CeO_2 catalysts with different platinum loadings were tested for the WGS reaction after an oxidative pretreatment at 500 °C. H_2 and CO_2 were the only products detected. No CH_4 production was observed in our reaction conditions (P=1 bar, T=230 °C), confirming the high selectivity of Pt/CeO_2 catalysts for LTS [41]. Interestingly, CO_2/H_2 molar ratios significantly higher than 1 were measured during the first 5 minutes of the reaction (Figure S5), which can be explained by the reduction of both PtO_x and ceria induced by CO. As shown in Table S2, the CO_2 overproduction (production added to that of the WGS reaction) significantly surpasses the production related to the reduction of PtO to Pt^0. This observation unveils a high reduction rate of CeO_2 and hence the presence of a high amount of oxygen vacancies and Ce^{3+} cations on the surface of CeO_2. Furthermore, the H_2 productivity strongly increased during the first few minutes reaching a maximal value and then slightly decreased (Figure S5).

The evolution of the molar activity as a function of Pt content is plotted in Figure 5 for the maximal value and after 45 min on stream.

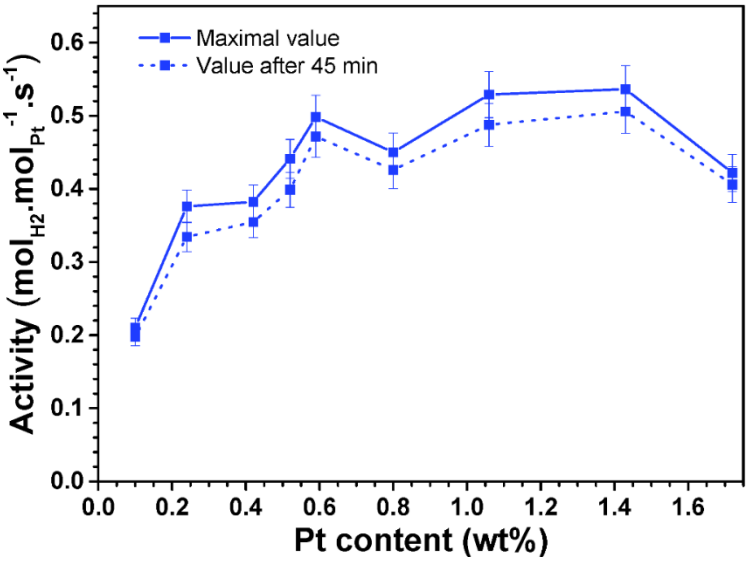

Figure 5. Influence of Pt loading on the maximal molar activity and after 45 min of Pt/CeO_2 catalysts for the WGS reaction after oxidative pretreatment at 500 °C. Reaction conditions: T=230 °C, $H_2O/CO/Ar/He$:33.3/8.3/54.2/4.2, GFSV = 600 $mL.min^{-1}.g^{-1}$.

It strongly increases between 0.10 and 0.59 wt% of Pt (0.02-0.12 $Pt.nm^{-2}$) from 0.2 to 0.5 $mol_{H2}.mol_{Pt}^{-1}.s^{-1}$ and afterward is relatively constant up to 1.43 wt% (0.35 $Pt.nm^{-2}$). Finally, a slight and slow decrease in activity is observed for each loading (Figures S5 and 5), which could be due to platinum sintering [40], ceria overreduction [41] or carbonate-induced poisoning [29,30].

3.3. Characterization after WGS reaction tests

The stability of the ceria support in the Pt/CeO_2 catalysts under the reaction conditions was evaluated through its crystallite size determined from XRD diffractograms (Figure S6a): it is 7-8 nm for the 1.06Pt catalyst, as the value before reaction. Furthermore, the F_{2g} bandwidths are identical (24 cm^{-1}) in the Raman spectra of fresh and spent 0.52Pt catalyst (Figure S6b), confirming the structural stability of the CeO_2 nanocrystallites. Finally, no significant change in the S_{BET} value was evidenced, both for the CeO_2 support and the 0.80Pt catalyst (Table S1). Thus, the slight deactivation of the catalysts observed after 45 min on stream is not due to a textural or structural change of the ceria support.

STEM-ADF images of the catalysts after reaction show the presence of Pt NPs whatever the loading (Figures 6a-d). For a Pt loading higher than 0.42 wt%, the number of observed particles was high enough for statistical analysis, leading to an average diameter of 1.4 nm with a standard deviation of 0.3 nm (Figure S7a). Interestingly, this value is almost constant with Pt content and consistent with the 1-2 nm particle size reported in the literature under reaction conditions [16]. However, it is likely that unobservable small clusters as well as SAs were also present in minority on the ceria surface.

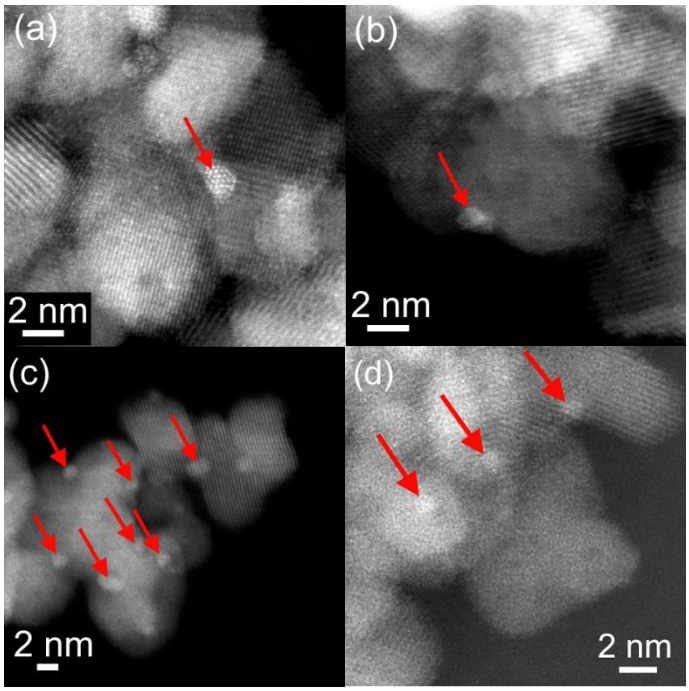

Figure 6. STEM-ADF images recorded with a Titan ETEM G2 80-300 kV (FEI) microscope of (a) 0.52Pt, (b) 0.80Pt, (c) 1.06Pt and (d) 1.72Pt after testing under WGS reaction feed at 230 °C for 4 h. Red arrows point to Pt NPs.

The XRD diffractogram of 1.06Pt catalyst contains a diffraction peak at 39.7° after reaction (Figure S7b), significantly higher than the noise level contrary to the fresh state (Figure 1). Consequently, Pt cations are reduced and agglomerated enough to crystallize in reaction conditions.

XPS spectra of spent catalysts (Figure S8) also reveal that the presence of Pt^0 atoms at the surface persists despite air exposure after WGS reaction. Furthermore, a second component attributed to Pt^{2+} cations can be distinguished in the spectra suggesting that some Pt species either were not reduced during the WGS reaction or were easily reoxidized upon air exposure. Interestingly, the relative proportion of Pt^{2+} species was higher for 0.25Pt compared to 0.80Pt: 0.25Pt exhibits 71% of Pt^0 and 29% of Pt^{2+}, while for 0.80Pt, the surface contains 77% and 23% of Pt^0 and Pt^{2+}, respectively.

MicroRaman spectra recorded on the spent catalysts show a strong decrease in the relative intensity of the $\nu(PtO_x)$ band at 660-685 cm^{-1} (Figure 7a), suggesting a reduction of Pt^{2+} cations [29] in agreement with XRD and XPS. The remaining $\nu(PtO_x)$ feature may result either from the reoxidation of Pt^0 atoms in ambient air or the presence of Pt^{2+} cations that were not reduced during the reaction. As a matter of fact, this feature is poorly affected by the Pt loading, which

makes us attribute it to Pt^{2+} cations strongly anchored on CeO_2. Note that the reduction of 0.9%Pt/CeO_2 catalyst under H_2 at 500 °C led to the complete disappearance of this band [29]. Furthermore, the ν(O-O) band at 826 cm^{-1} was enhanced, revealing a larger amount of peroxo species on the surface of catalysts. Those species, which arise from the reduction of chemisorbed O_2 molecules on oxygen vacancies, could be located at the interface between Pt and CeO_2.

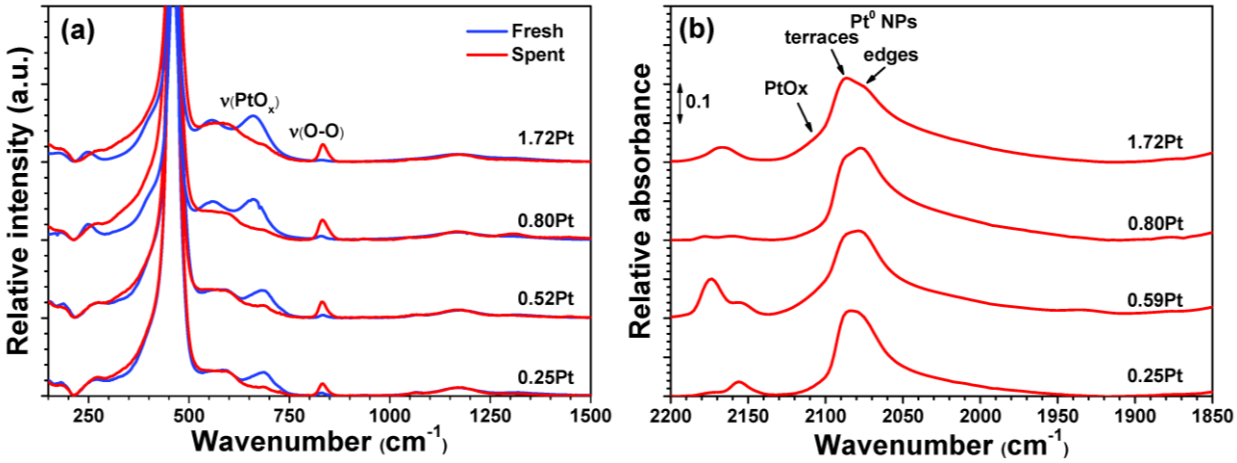

Figure 7. Comparison of (a) Raman spectra in the fresh and spent states for different Pt loadings and (b) CO-DRIFT spectra of spent catalysts recorded between 1850 and 2200 cm^{-1} at 0 °C under a 2% CO/He flow and normalized on the band at 2088 cm^{-1}, the backgrounds correspond to the spectra of pretreated samples recorded at the same temperatures and the $\nu(CO)_{gas}$ signal is subtracted.

Two main bands located at 2088 and 2078 cm^{-1} can be distinguished in the CO-DRIFT spectra of the spent catalysts recorded at 20 °C (Figure 7b). They were attributed to CO linearly chemisorbed on terraces [23,37,44,45] and step/edge sites [37,44] of Pt^0 NPs. Shoulders are also observed near 2107 and 2056 cm^{-1}. These features were attributed to PtO_x clusters and corner sites of Pt^0 or $Pt^{\delta+}$ NPs, respectively [37,44]. As for the fresh catalysts, formation of bidentate and hydrogen carbonates was observed during such measurements (Figure S9).

3.4. CO-TPR analysis

Figure S10 displays the CO consumption and CO_2 production profiles during CO-TPR analysis achieved between 20 °C and 500 °C for CeO_2 and the series of Pt/CeO_2 catalysts. As shown in Figure 8, a significant decrease in the temperature of maximal CO consumption is observed consistently with the literature [46], especially for Pt content lower than 0.25 wt%. For high Pt loading, consumption of CO begins already at RT due to the formation of carbonyls and carbonates. Furthermore, both the onset temperature and the temperature of maximal CO_2

production decrease strongly with increasing Pt content (Figure S11). Indeed, O^{2-} anions of PtO_x and CeO_2 become more labile leading to CO_2 desorption at lower temperature. A similar trend was reported by Boronin *et al.* for Pt contents from 1 to 20 wt% [47].

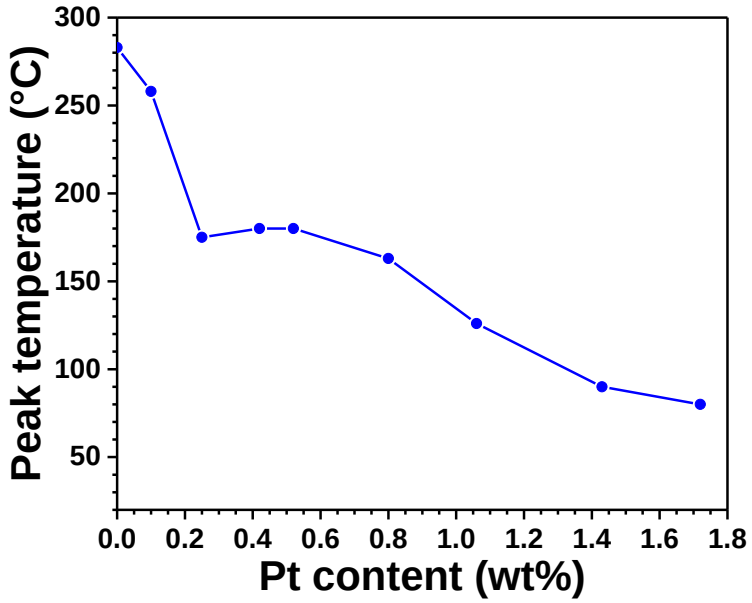

Figure 8. Evolution with the Pt content of the temperature of maximal CO consumption determined from CO-TPR curves.

In fact, the CO_2 production profile can originate from various phenomena such as the reduction of PtO_x species (Eq.1), the reduction of surface anionic layers of CeO_2 (Eq. 2, the square represents an oxygen vacancy), the WGS reaction with the hydroxyl groups present on the surface (Eq. 3), and the Boudouard reaction (Eq. 4) [48,49].

$$PtO + CO \rightarrow Pt^0 + CO_2 \qquad (Eq.\ 1)$$

$$CO + O^{2-}(support) \rightarrow CO_2 + \square(support) + 2e^- \qquad (Eq.\ 2)$$

$$CO + 2OH^-(support) \rightarrow CO_2 + H_2 + O^{2-}(support) \qquad (Eq.\ 3)$$

$$2CO \rightarrow CO_2 + C \qquad (Eq.\ 4)$$

In most works using CO-TPR analysis, it has been shown that the deposition of carbon on the surface is negligible below 500 °C [49–51], thus the Boudouard reaction can be ruled out for our study. A CO_2 production peak at 400-500 °C is accompanied by H_2 production and can be attributed to the WGS reaction (see the H_2 signal intensity in Figure S12). Therefore, the peaks below 400 °C arise from the reduction of PtO_x species and CeO_2. However, as the CO consumption required to reduce the overall amount of PtO to Pt^0 is much lower than the measured one (Table S3), the peaks reveal mostly reduction of ceria, which implies that its

reducibility strongly increases with Pt content. It is particularly highlighted by the evolution of CO consumption (Figure 8). Furthermore, the total CO consumption is rather constant (450- 550 $\mu mol.g^{-1}$) for Pt content lower than 1.43 wt%, Table S3). Therefore, this parameter which is related to the reduction degree of ceria at 500 °C cannot explain the observed evolution of the catalytic activity as a function of Pt content (Figure 5).

Hence, the CO-TPR analyses show that the reducibility of the Pt/CeO_2 catalysts increases with Pt content. As the amount of PtO_x clusters also increases with Pt content, it suggests that Pt^0 particles are easier formed from PtO_x clusters instead of SAs. A higher number of formed Pt^0 particles also favors consecutive reduction of CeO_2. Moreover, oxygen vacancies are often defined either as the active sites for water dissociation leading to H_2 production [16,52] or undergoing dissociative adsorption and forming Ce^{4+}-OH species as active participants [20]. Thus, an increase in the lability of oxygen vacancies may explain the increase in activity.

3.5. CO-TPR followed by *in situ* DRIFT spectroscopy

To gain a better understanding of the structural evolution of Pt species and surface species formed during CO-TPR experiments, DRIFT spectra were recorded under CO at increasing temperatures from 5 to 279 °C (Figure 9). No significant band was observed below 2100 cm^{-1} for CeO_2 support (Figure 9a). For Pt/CeO_2 catalysts (Figures 9b-d), ν(CO) bands are observed in the ranges 2090-2100 cm^{-1}, 2070-2075 cm^{-1} and 2050-2060 cm^{-1}, which are attributed to CO molecules chemisorbed linearly on PtO_x clusters, terraces and edges of Pt^0 NPs, respectively [23,37,44,45].

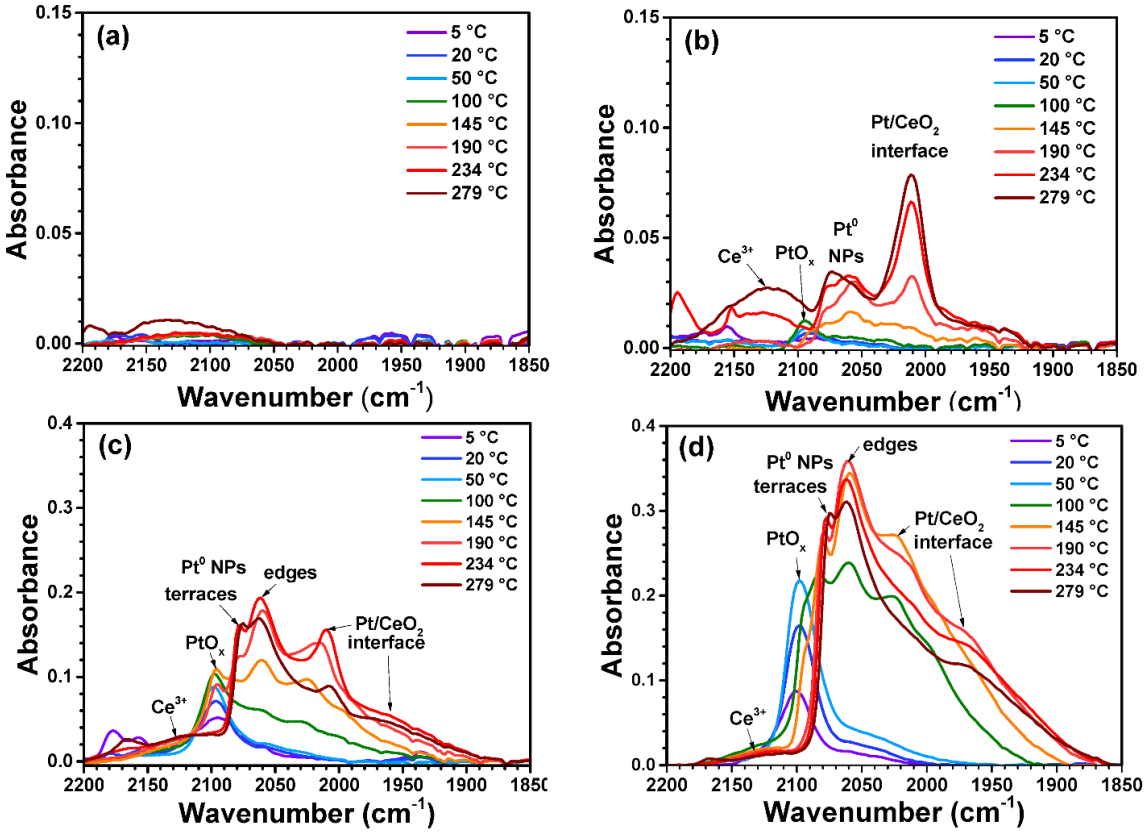

Figure 9. CO-DRIFT spectra between 1850 and 2200 cm^{-1} of (a) CeO_2, (b) 0.10Pt (c) 0.52Pt and (d) 1.72Pt catalysts recorded at different temperatures under 2%CO/He. The backgrounds correspond to the spectra of KBr powder recorded at the same temperatures and the $\nu(CO)_{gas}$ signal is subtracted.

A red shift of ca 10-20 cm^{-1} is observed during CO-TPR compared to CO chemisorption at RT which is mainly due to the difference of temperature, as shown in Figure S13. Less clearly, the band at 2010-2020 cm^{-1} was attributed to CO species linearly adsorbed on very small Pt particles mainly populated by very low coordination sites [53], or to CO linearly adsorbed on perimeter Pt sites [16], to CO adsorbed on Pt-Ce interface [22] while the one at 1950-1970 cm^{-1} was assigned to CO adsorbed on very low coordinated Pt atoms in strong interaction with the support [53], to CO adsorbed on platinum atoms interacting with Ce^{3+} cations [54], or to a bridged CO adsorption at the metal-support interface [16]. Therefore, both bands were attributed to CO species adsorbed at the interface. Interestingly, the species characterized by the band at 1950-1970 cm^{-1} give rise to that at 2010-2020 cm^{-1} when the interaction of CO with CeO_2 is prevented [53].

The band of PtO_x clusters at 2090-2100 cm^{-1} appears at ambient temperature for the 0.52Pt and 1.72Pt catalysts (Figure 9b and c) and between 50 and 100 °C for 0.10Pt (Figure 9a).

The high stability of SAs on the surface of the latter catalyst may explain the formation of PtO_x clusters only at higher temperatures in accordance with the literature [31]. As shown by the amplitude evolution at 2098 and 2078 cm^{-1} in Figure S14, the band of PtO_x species increases and then gradually disappears as the band of Pt^0 terraces increases. This clearly shows the agglomeration of PtO_x, followed by its reduction to Pt^0 NPs. Furthermore, the temperature required for transformation of Pt species increases with decreasing the Pt content. Indeed, the disappearance of the band at 2090-2100 cm^{-1} and the appearance of the bands at 2070-2075 cm^{-1} and 2050-2060 cm^{-1}, begin at 50 °C for the 1.72Pt catalyst, at 100-150 °C for 0.52Pt and 0.10Pt. Those temperatures coincide with the onset temperatures of CO_2 production (Figure S11), showing that the formation of Pt^0 NPs favors the reduction of CeO_2.

The relative absorbance of the bands at 2050-2060 cm^{-1} (Pt^0 NPs edges) and 2010-2020 cm^{-1} (Pt/CeO_2 interface) increases as the Pt content decreases, with a main band at 2012 cm^{-1} for the 0.10Pt catalyst. For the 0.52Pt and 1.72Pt catalysts, the spectral evolution with temperature clearly shows the agglomeration of Pt atoms with the disappearance of the band at 2010-2020 cm^{-1}. The maximal absorbance of this band is at 279 °C or above for the 0.10Pt catalyst, at 234 °C for 0.52Pt, and at 100 °C for 1.72Pt. Hence, Pt dispersion and resistance to agglomeration increase while decreasing the Pt content. As soon as the band at 2010 cm^{-1} disappears, a band at 1930 - 1980 cm^{-1} appears, in agreement with the literature [53]. Its absorbance is higher at 279 °C for the 1.72Pt catalyst because of higher reducibility. The reduction of ceria, which leads to formation of Ce^{3+} cations, is evidenced by the appearance of the broad band at 2120 cm^{-1} corresponding to the $^2F_{5/2} \rightarrow {}^2F_{7/2}$ electronic transition of Ce^{3+} cations [31,57] and not to a ν(CO) stretching vibration. Interestingly, the appearance of this band correlates with the onset of CO_2 production observed during the CO-TPR analysis (Figure S15).

The analysis of the other spectral ranges unveiled modifications of surface species during CO-TPR even at 5 °C. Indeed, new bands attributed to bidentate carbonates were observed at 1290 and 1585 cm^{-1} (Figure S16) in addition of bands of monocarbonates at 1390 and 1470 cm^{-1} [37]. Furthermore, the bands appearing at 1220, 1390 and 1525 cm^{-1} which arose from formation of hydrogen carbonates (bicarbonates) [37] disappeared upon increasing the temperature: the higher the platinum content, the lower the temperature of appearing and disappearing. Finally, formation of formates at higher temperatures was revealed by the raise of bands at 2950, 2840 and 2715 cm^{-1} (Figure S17) which were attributed to a combination of δ(C-H) and ν_{as}(OCO)

vibrations, ν(C-H) vibrations and a combination of δ(C-H) and ν_s(OCO) vibrations, respectively [38,55]. The latter could alternatively correspond to the overtone of the δ(C-H) band [37,38]. Again, the temperature at which the bands raise decreases with increasing Pt content.

Furthermore, four bands are observed at 3712, 3688, 3662 and 3505 cm^{-1} after the pretreatment at 500 °C compared to the fresh ceria, in the same proportions for all Pt contents (Figure S18). The first one was attributed to ν(OH) vibrations of terminal OH (type I) [56], the two following ones to bridging OH with two cerium atoms (type II-A) [43,44] and the last one to tridentate OH [37] and hydrogen-bonded terminal OH [57]. An attribution of the main band at 3662 cm^{-1} to ν(H_2O) vibration of chemisorbed water can be ruled out since it is not associated with the observation of δ(H_2O) band around 1630 cm^{-1}. Upon CO adsorption at 5 °C, the ν(OH) bands were unchanged (Figure S19). However, the main band was shifted from 3660 to 3640 cm^{-1} during the temperature rise (Figure S19) which was attributed to formation of bridging hydroxyls neighbored by oxygen vacancies and Ce^{3+} cations (type II-B OH) [37,56]. The shift occurs at lower temperatures as Pt content increases (Figure 10), confirming that reducibility of CeO_2 increases with Pt content.

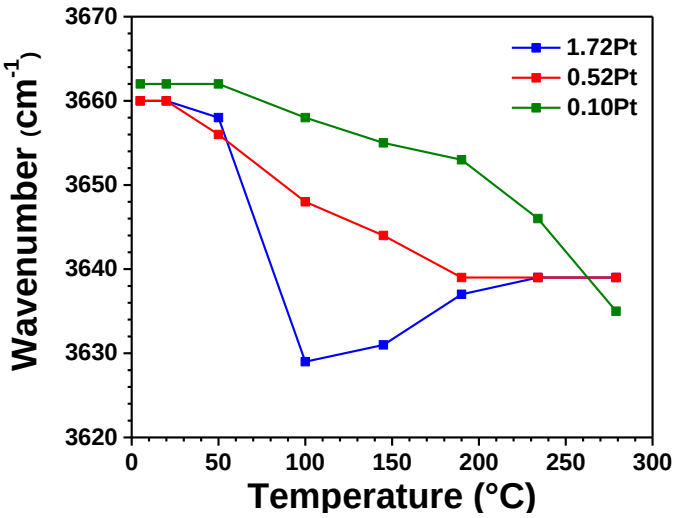

Figure 10. Evolution of the wavenumber of the ν(O-H) band of type II OH species as a function of temperature during CO-TPR followed by *in situ* DRIFT spectroscopy.

Summarizing, DRIFT spectra recorded during CO-TPR show an increase in the number of PtO_x clusters with Pt content, probably formed from the agglomeration of SAs. PtO_x clusters are then easily aggregated and reduced by CO to form Pt^0 NPs, leading to a reduction of the CeO_2 surface and evolution of surface species. Consequently, the increase in Pt molar activity from

0.10 to 0.59 wt% of Pt (Figure 5) could be explained by the increase in the quantity of Pt^0 particles formed on the surface of catalysts under reaction conditions. To prove this assumption, *operando* DRIFT measurements were undertaken.

3.6. *Operando* DRIFT spectroscopy

As the H_2O and CO molar concentrations used for *operando* measurements (2 and 0.5%, respectively) were lower than those used for standard catalytic testing, it was important to check that the same trends of catalytic properties were obtained. As expected, the evolution of molar activity plotted as a function of the Pt content in Figure S20 shows a strong increase (factor 3) from 0.1 to ca 0.6 wt% of Pt, similarly to standard catalytic testing, though with a sharp optimum.

DRIFT spectra of the catalysts recorded after oxidative pretreatment at 500 °C clearly show a decrease in the absorbance of the ν3 bands of carbonates between 800 and 1800 cm^{-1} and physisorbed water between 3000 and 3500 cm^{-1} (Figure S18) compared to the fresh state. The *operando* spectra recorded at the stationary WGS state show the formation of carbonyl species (Figure 11a) identical to those observed during CO-TPR analysis (Figure 9). Indeed, the spectra of the 0.42Pt, 0.52Pt, 0.59Pt, 1.06Pt, and 1.43Pt catalysts reveal the presence of CO species chemisorbed on the terraces and edges of Pt^0 particles (bands at 2065-2072 cm^{-1} and 2045-2056 cm^{-1}, respectively) as well as CO species at the Pt-CeO_2 interface (bands at 2008-2020 and near 1960 cm^{-1}). Moreover, no signal of carbonyl species was observed for the 0.10Pt catalyst and is quite loose for 0.25Pt. To make a semi-quantitative comparison of the carbonyl bands, the DRIFT spectra were normalized to the band at 2065-2072 cm^{-1} (Figure 11a): for Pt contents below 0.59 wt%, a higher relative absorbance of the ν(CO) bands at 2045-2056 cm^{-1} and 2008-2020 cm^{-1} is observed, indicating an increase in the quantity of edge sites and Pt atoms at the interface due to the smaller size of Pt^0 NPs. For Pt content above 0.59 wt%, Pt^0 NPs with a similar IR spectral signature are found on the surface of the catalysts. Furthermore, the broad band at 2125 cm^{-1} attributed to the presence of Ce^{3+} cations [31,58] is observed (Figure 11a), demonstrating the reduction of CeO_2 in reaction conditions. Note that no broad signal was observed at this wavenumber for the *ex situ* analysis of the spent catalysts (Figure 7b) due to reoxidation of CeO_2 in ambient air.

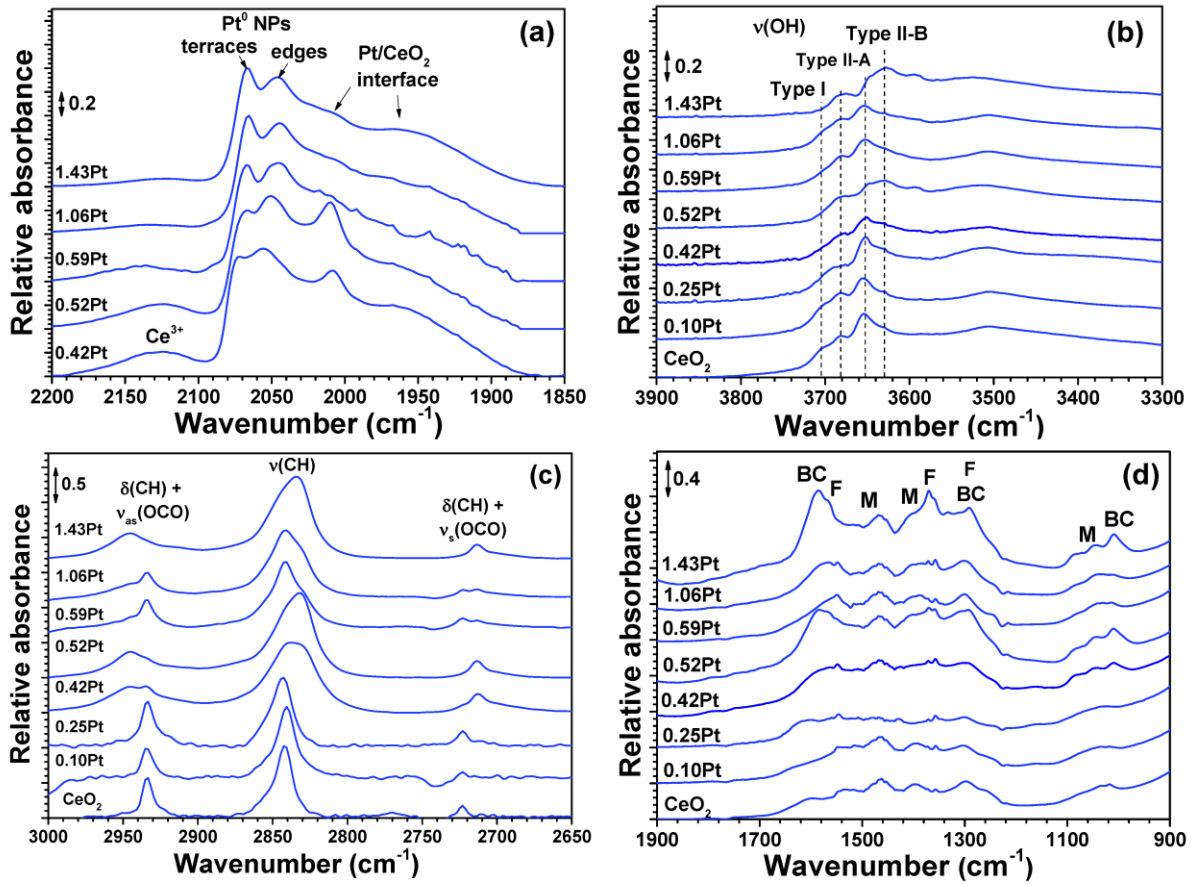

Figure 11. *Operando* DRIFT spectra of Pt/CeO_2 catalysts during WGS reaction for different Pt loadings: (a) 1850-2200 cm^{-1} region normalized on the band at 2065-72 cm^{-1}, (b) 3300–3900 cm^{-1} region, (c) 2650-3000 cm^{-1} region normalized on the band at 2842 cm^{-1} and (d) 900-1900 cm^{-1} region. BC: bidentate carbonate, M: monodentate carbonate, F: formate. Reaction conditions: T=230 °C, H_2O/CO/He: 2.0/0.5/97.5, GHSV =1000 $mL.min^{-1}.g^{-1}$. The backgrounds correspond to the spectra of KBr powder recorded at the same temperatures and the $\nu(CO)_{gas}$ signal is subtracted.

Characterization of hydroxyl species is essential for the WGS reaction since some of them are involved in the reaction mechanism [16]. The ν(O-H) band observed near 3680 cm^{-1} during reaction was attributed either to bridging OH (type II-A) on the surface of reduced ceria [16,38,56,57] or to chemisorbed water [38,56,57]. However, as it was also observed near 230 °C during CO-TPR, the first attribution was preferred. Furthermore, ν(OH) band due to type II-B OH can be distinguished at 3620-3640 cm^{-1} [37,38] especially at high Pt content confirming reduction of ceria.

For all catalysts, typical bands of bidentate formate species appear under reaction conditions at 2935-2944, 2831-2842 and 2713-2723 cm^{-1} (Figure 11c). Below 0.42 wt% of Pt, only the

bands at 2935, 2842 and 2723 cm^{-1} corresponding to bidentate formates adsorbed on the surface of CeO_2 are observed, similarly to Vignatti *et al.* [59]. At higher Pt content, the spectra contain bands at 2944, 2831 and 2713 cm^{-1} due to formates bridged with two Ce atoms [37].

For all the catalysts, a bidentate carbonate giving rise to ν_3 bands at 1519 and 1228 cm^{-1} and ν_1 band at 1033 cm^{-1} after pretreatment was consumed from the beginning of reaction (Figure S21) [38,39]. The bands at 1290-1330, 1360-1370 cm^{-1} and 1550-1560 cm^{-1} observed in reaction conditions correspond to the ν_s(OCO), δ(C-H) and ν_{as}(OCO) bands of formates, respectively [37,38,55]. Additionally, ν3 pairs of bands observed around 1300/1590 cm^{-1} and 1395/1460 cm^{-1} are assigned to bidentate and either monodentate or polydentate carbonates, respectively [37,38,60–63]. However, no significant difference between the different Pt/CeO_2 catalysts appears in this spectral region (Figure 11d).

To gain understanding on the reaction mechanism, the temporal evolution of DRIFT spectra of 0.42Pt after CO removal from the reaction feed is plotted in Figure S22. It clearly shows a rapid disappearance without any shift of the band at 2012 cm^{-1} (Figure S22a) suggesting that the interface is involved in the reaction mechanism. The spectral evolution between 2020 and 2090 cm^{-1} is difficult to interpret since it combines red-shift of bands due to a dipole-dipole interaction between CO and H_2O or a modification of the charge transfer between the NP and the $2\pi^*$ orbital of CO by the modification of the NP potential with the interaction of water [16]. Furthermore, bridging formates disappear when CO is removed from the gas phase (Figure S22c) while bidentate formates appear to be unaffected suggesting that the former could be reaction intermediates. Finally, no significant spectral change is observed for the hydroxyl and carbonates species (Figures S22b and S22d, respectively).

In summary, a reduction of PtO_x clusters to Pt^0 particles under reaction conditions was demonstrated by *operando* DRIFT spectroscopy as well as a reduction of CeO_2. For high Pt contents (>0.59 wt%), reduction and agglomeration lead to the formation of Pt^0 NPs with a similar spectral signature. In contrast, spectra of catalysts with Pt loading below 0.52 wt% show the presence of Pt particles with lower nuclearity. Bridging formates could be reaction intermediates formed at the interface between reduced CeO_2 and Pt^0 NPs.

4. Discussion

The influence of the Pt loading on the catalytic activity of Pt/CeO_2 catalysts was previously investigated by several groups. However, different trends were reported depending on the fresh state of the catalyst, the pre-treatment applied and the reaction conditions [14,24,25,64]. In the present work, an oxidizing pretreatment at 500 °C was applied to produce ultradispersed PtO_x species, in the continuity of previous studies [29,31,65]. An increase in activity by a factor of 2.5 was evidenced when increasing the Pt loading from 0.1 to 0.6 wt%, reaching a plateau from 0.6 to 1.4 wt%. Such evolution has never been reported in the literature before.

As several Pt species can coexist at the surface of Pt/CeO_2 catalysts and as different structural modifications can occur depending on the reaction conditions, it could be difficult to determine the active sites [20,23,66,67]. However, the evolution of the Pt molar activity as a function of Pt content allows us to conclude that the PtO_x SAs and clusters and Pt^0 NPs own very different intrinsic activities. Indeed, formation of NPs with diameter of ca 1.4 nm during the WGS reaction was revealed by STEM-ADF for Pt loading of 0.52 wt% and above. It agrees with Jacobs *et al.* who, even for a high loading around 5 wt%, observed the formation of NPs between 1 and 2 nm at 250 °C [25] and with Li *et al.* who similarly observed the formation of 1.4 nm NPs after reaction at 300 °C, starting with a 1 wt% catalyst composed essentially of SAs [20]. Furthermore, *operando* DRIFT spectra clearly showed that these NPs contain metallic Pt^0 atoms and are interfaced with reduced CeO_2 support.

It supports that Pt^0 NPs are the most active species for the water-gas shift reaction [16–22]. Furthermore, the sequential experiment by removal of CO from the gas feed confirms that the active sites are located at the perimeter of the interface between the Pt^0 NPs and reduced CeO_2 [7,8,16,22].

Consequently, the plateau of molar activity (expressed in $mol_{H2}.mol_{Pt}^{-1}.s^{-1}$) suggests that the number of active sites at the interface is similar for all Pt^0 NPs of 1.4 nm, with only the number of interfaced Pt NPs varying with loading. Note that the molar activity is then proportional to the turnover frequency (TOF) but much lower. Furthermore, even if PtO_x SAs or small clusters strongly anchored to CeO_2 and hardly reducible could coexist with Pt^0 NPs at high Pt loading, their contribution to the overall activity appears to be negligible to obtain a plateau. Conversely, these species predominate at low loading, leading to a much lower molar activity (corresponding to a TOF value in this case). This finding is in agreement with the recent thesis of X. Li reporting

almost zero activity for Pt SAs [20] but might appear in contradiction with the conclusions of Flytzani-Stephanopoulos group [13,14]. However, Pt cationic species were obtained using a sodium cyanide leaching method to remove Pt^0 NPs and the activity could be modified by the presence of alkali actions associated with OH surface groups [9,68].

Therefore, the Pt surface content is a key parameter for the formation of active species for the water-gas shift reaction at low temperatures as also demonstrated for CO oxidation [23]. The loading has to be high enough to form PtO_x clusters which are easily agglomerated and reduce to the Pt^0 NPs under reaction conditions. This minimal loading could depend on the number of sites able to strongly anchor PtO_x SAs and small clusters which are hardly reduced and poorly active for the WGS reaction. As the surface defects of ceria act as anchoring sites [13,19,20,69–72], the preparation method and thermal treatments of Pt/CeO_2 catalysts could influence it.

5. Conclusion

A series of Pt/CeO_2 catalysts was prepared to investigate the influence of the Pt loading (0.1 to 1.72 wt%) on the water-gas shift reaction rate at 230 °C. An oxidizing treatment at 500 °C was applied before testing to stabilize ultradispersed Pt species. At the fresh state, the absence of nanosized Pt^0 particles (>1 nm) was confirmed for Pt contents below 1.72 wt%. Pt SAs were predominantly present in the catalyst containing 0.10 wt% Pt. Above 0.25 wt%, microRaman spectroscopy revealed the presence of PtO_x species, Both PtO_x SAs and small clusters were observed by STEM at high loading.

It was shown that the Pt-molar activity strongly increases up to 0.6 wt% and is rather constant thereafter. A reduction of PtO_x clusters to Pt^0 NPs of ca 1.4 nm followed by a reduction of CeO_2 surface occurs under reaction conditions. According to CO-TPR analysis and *operando* DRIFT measurements, for Pt contents below 0.6 wt%, Pt species possess a lower nuclearity and seem to be in strong interaction with CeO_2. Their low reducibility limits their activation under reaction mixture and, consequently, their catalytic activity. Conversely, the higher activity for Pt contents above 0.6 wt% is related to the easy formation of Pt^0 NPs of ca 1.4 nm under reaction conditions, which are more active than Pt clusters and do not evolve in intrinsic activity as a function of Pt loading. The plateau of Pt-molar activity arises from an increase in the number of Pt^0 NPs without sintering. The structural change between the fresh Pt/CeO_2 state and that under reaction conditions is therefore highly dependent on the Pt content. Hence, the molar catalytic

activity of Pt/CeO_2 for WGS can be optimized through the Pt loading, and it could be further improved by an optimal treatment aiming at shaping the most active species through the interaction of Pt with ceria.

Acknowledgement

The authors gratefully acknowledge Vincent Collière from Laboratoire de Chimie de Coordination (CNRS Toulouse) for performing High Resolution Electron Microscopy at Centre Castaing. The Lyon Doctoral School of Chemistry (ED206) is acknowledged for the scholarship of C. Molinet-Chinaglia. This work was supported by the French National Research agency (Agence Nationale de la Recherche (ANR)) in the framework of the DYCAT project (ANR-19-CE05-0038).

Graphical abstract

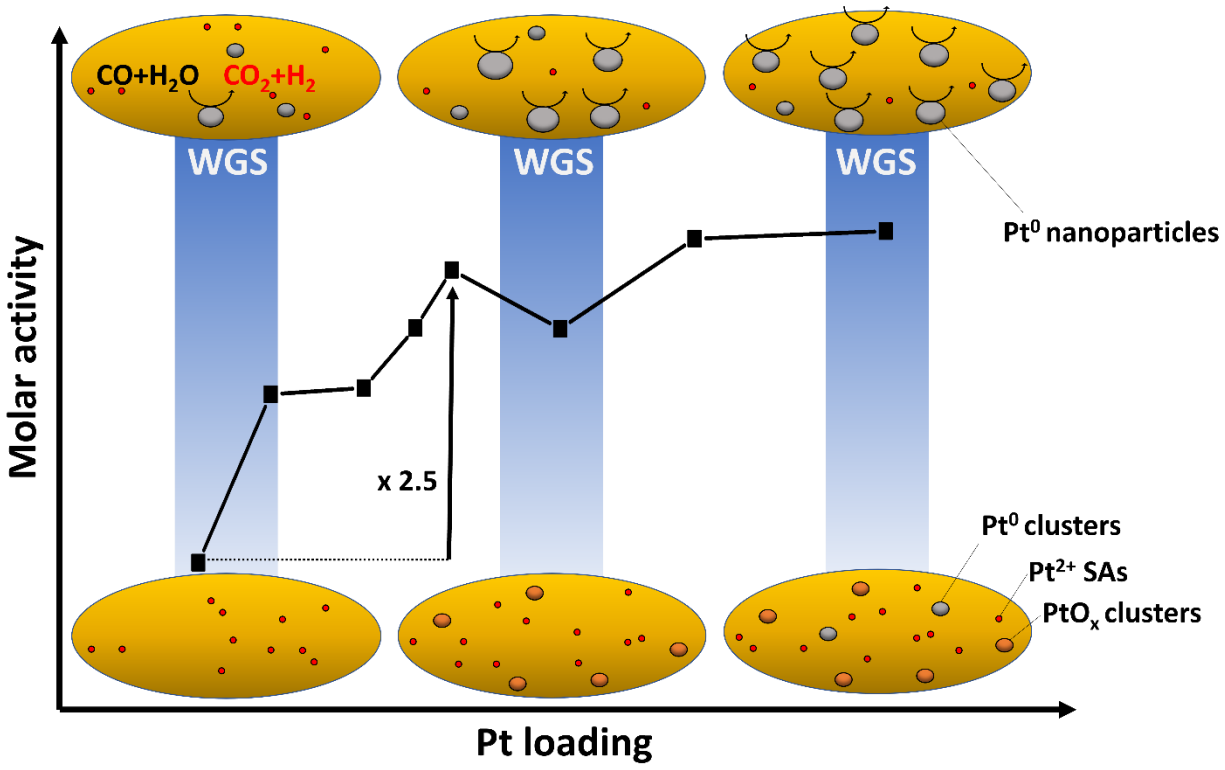

References

[1] C. Ratnasamy, J.P. Wagner, Water Gas Shift Catalysis, Catal. Rev. 51 (2009) 325–440. https://doi.org/10.1080/01614940903048661.

[2] L. Gradisher, B. Dutcher, M. Fan, Catalytic hydrogen production from fossil fuels via the water gas shift reaction, Appl. Energy 139 (2015) 335–349. https://doi.org/10.1016/j.apenergy.2014.10.080.

[3] H.-S. Roh, D.-W. Jeong, K.-S. Kim, I.-H. Eum, K.Y. Koo, W.L. Yoon, Single Stage Water–Gas Shift Reaction Over Supported Pt Catalysts, Catal. Lett. 141 (2011) 95–99. https://doi.org/10.1007/s10562-010-0480-3.

[4] P. Panagiotopoulou, J. Papavasiliou, G. Avgouropoulos, T. Ioannides, D.I. Kondarides, Water–gas shift activity of doped Pt/CeO2 catalysts, Chem. Eng. J. 134 (2007) 16–22. https://doi.org/10.1016/j.cej.2007.03.054.

[5] O. Thinon, F. Diehl, P. Avenier, Y. Schuurman, Screening of bifunctional water-gas shift catalysts, Catal. Today 137 (2008) 29–35. https://doi.org/10.1016/j.cattod.2008.01.001.

[6] C.M. Kalamaras, I.D. Gonzalez, R.M. Navarro, J.L.G. Fierro, A.M. Efstathiou, Effects of Reaction Temperature and Support Composition on the Mechanism of Water–Gas Shift Reaction over Supported-Pt Catalysts, J. Phys. Chem. C 115 (2011) 11595–11610. https://doi.org/10.1021/jp201773a.

[7] S. Aranifard, S.C. Ammal, A. Heyden, On the Importance of the Associative Carboxyl Mechanism for the Water-Gas Shift Reaction at Pt/CeO_2 Interface Sites, J. Phys. Chem. C 118 (2014) 6314–6323. https://doi.org/10.1021/jp5000649.

[8] S. Aranifard, S.C. Ammal, A. Heyden, On the importance of metal–oxide interface sites for the water–gas shift reaction over Pt/CeO_2 catalysts, J. Catal. 309 (2014) 314–324. https://doi.org/10.1016/j.jcat.2013.10.012.

[9] Y. Zhai, D. Pierre, R. Si, W. Deng, P. Ferrin, A.U. Nilekar, G. Peng, J.A. Herron, D.C. Bell, H. Saltsburg, M. Mavrikakis, M. Flytzani-Stephanopoulos, Alkali-Stabilized Pt-OHx Species Catalyze Low-Temperature Water-Gas Shift Reactions, Science 329 (2010) 1633–1636. https://doi.org/10.1126/science.1192449.

[10] J. Vecchietti, A. Bonivardi, W. Xu, D. Stacchiola, J.J. Delgado, M. Calatayud, S.E. Collins, Understanding the Role of Oxygen Vacancies in the Water Gas Shift Reaction on Ceria-Supported Platinum Catalysts, ACS Catal. 4 (2014) 2088–2096. https://doi.org/10.1021/cs500323u.

[11] A.M. Efstathiou, Elucidation of mechanistic and kinetic aspects of water–gas shift reaction on supported Pt and Au catalysts via transient isotopic techniques, (2016). https://doi.org/10.1039/9781782626855-00175.

[12] C.M. Kalamaras, S. Americanou, A.M. Efstathiou, "Redox" vs "associative formate with –OH group regeneration" WGS reaction mechanism on Pt/CeO_2: Effect of platinum particle size, J. Catal. 279 (2011) 287–300. https://doi.org/10.1016/j.jcat.2011.01.024.

[13] Q. Fu, H. Saltsburg, M. Flytzani-Stephanopoulos, Active Nonmetallic Au and Pt Species on Ceria-Based Water-Gas Shift Catalysts, Science 301 (2003) 935–938. https://doi.org/10.1126/science.1085721.

[14] D. Pierre, W. Deng, M. Flytzani-Stephanopoulos, The Importance of Strongly Bound Pt–CeO_x Species for the Water-gas Shift Reaction: Catalyst Activity and Stability Evaluation, Top. Catal. 46 (2007) 363–373. https://doi.org/10.1007/s11244-007-9013-8.

[15] R. Tiwari, B. Sarkar, R. Tiwari, C. Pendem, T. Sasaki, S. Saran, R. Bal, Pt nanoparticles with tuneable size supported on nanocrystalline ceria for the low temperature water-gas-shift (WGS) reaction, J. Mol. Catal. Chem. 395 (2014) 117–123. https://doi.org/10.1016/j.molcata.2014.08.021.
[16] Y. Li, M. Kottwitz, J.L. Vincent, M.J. Enright, Z. Liu, L. Zhang, J. Huang, S.D. Senanayake, W.-C.D. Yang, P.A. Crozier, R.G. Nuzzo, A.I. Frenkel, Dynamic structure of active sites in ceria-supported Pt catalysts for the water gas shift reaction, Nat. Commun. 12 (2021) 914. https://doi.org/10.1038/s41467-021-21132-4.
[17] C.M. Kalamaras, D.D. Dionysiou, A.M. Efstathiou, Mechanistic Studies of the Water–Gas Shift Reaction over $Pt/Ce_xZr_{1-x}O_2$ Catalysts: The Effect of Pt Particle Size and Zr Dopant, ACS Catal. 2 (2012) 2729–2742. https://doi.org/10.1021/cs3006204.
[18] M. Gonzalez Castaño, T.R. Reina, S. Ivanova, M.A. Centeno, J.A. Odriozola, Pt vs. Au in water–gas shift reaction, J. Catal. 314 (2014) 1–9. https://doi.org/10.1016/j.jcat.2014.03.014.
[19] T.R. Reina, M. Gonzalez-Castaño, V. Lopez-Flores, L.M. Martínez T, A. Zitolo, S. Ivanova, W. Xu, M.A. Centeno, J.A. Rodriguez, J.A. Odriozola, Au and Pt Remain Unoxidized on a CeO_2-Based Catalyst during the Water–Gas Shift Reaction, J. Am. Chem. Soc. 144 (2022) 446–453. https://doi.org/10.1021/jacs.1c10481.
[20] X. Li, Structure-Performance Relationship of Pt/CeO_2 Catalysts for the Water-Gas Shift Reaction, Doctoral Thesis, ETH Zurich, 2023. https://doi.org/10.3929/ethz-b-000620557.
[21] K. Ding, A. Gulec, A.M. Johnson, N.M. Schweitzer, G.D. Stucky, L.D. Marks, P.C. Stair, Identification of active sites in CO oxidation and water-gas shift over supported Pt catalysts, Science 350 (2015) 189–192. https://doi.org/10.1126/science.aac6368.
[22] K. Yuan, Y. Guo, Q.-L. Lin, L. Huang, J.-T. Ren, H.-C. Liu, C.-H. Yan, Y.-W. Zhang, Size effect-tuned water gas shift reaction activity and pathway on ceria supported platinum catalysts, J. Catal. 394 (2021) 121–130. https://doi.org/10.1016/j.jcat.2020.12.035.
[23] F. Maurer, A. Beck, J. Jelic, W. Wang, S. Mangold, M. Stehle, D. Wang, P. Dolcet, A.M. Gänzler, C. Kübel, F. Studt, M. Casapu, J.-D. Grunwaldt, Surface Noble Metal Concentration on Ceria as a Key Descriptor for Efficient Catalytic CO Oxidation, ACS Catal. 12 (2022) 2473–2486. https://doi.org/10.1021/acscatal.1c04565.
[24] I. Ivanov, P. Petrova, V. Georgiev, T. Batakliev, Y. Karakirova, V. Serga, L. Kulikova, A. Eliyas, S. Rakovsky, Comparative Study of Ceria Supported Nano-sized Platinum Catalysts Synthesized by Extractive-Pyrolytic Method for Low-Temperature WGS Reaction, Catal. Lett. 143 (2013) 942–949. https://doi.org/10.1007/s10562-013-1078-3.
[25] G. Jacobs, U.M. Graham, E. Chenu, P.M. Patterson, A. Dozier, B.H. Davis, Low-temperature water–gas shift: impact of Pt promoter loading on the partial reduction of ceria and consequences for catalyst design, J. Catal. 229 (2005) 499–512. https://doi.org/10.1016/j.jcat.2004.11.031.
[26] L. Piccolo, Restructuring effects of the chemical environment in metal nanocatalysis and single-atom catalysis, Catal. Today 373 (2021) 80–97. https://doi.org/10.1016/j.cattod.2020.03.052.
[27] K. Krupski, M. Moors, P. Jóźwik, T. Kobiela, A. Krupski, Structure Determination of Au on Pt(111) Surface: LEED, STM and DFT Study, Materials 8 (2015) 2935–2952. https://doi.org/10.3390/ma8062935.
[28] W. Lin, A.A. Herzing, C.J. Kiely, I.E. Wachs, Probing Metal−Support Interactions under Oxidizing and Reducing Conditions: In Situ Raman and Infrared Spectroscopic and Scanning Transmission Electron Microscopic−X-ray Energy-Dispersive Spectroscopic

Investigation of Supported Platinum Catalysts, J. Phys. Chem. C 112 (2008) 5942–5951. https://doi.org/10.1021/jp710591m.
[29] G. Ferré, M. Aouine, F. Bosselet, L. Burel, F.J.C.S. Aires, C. Geantet, S. Ntais, F. Maurer, M. Casapu, J.-D. Grunwaldt, T. Epicier, S. Loridant, P. Vernoux, Exploiting the dynamic properties of Pt on ceria for low-temperature CO oxidation, Catal. Sci. Technol. 10 (2020) 3904–3917. https://doi.org/10.1039/D0CY00732C.
[30] L. Nie, D. Mei, H. Xiong, B. Peng, Z. Ren, X.I.P. Hernandez, A. DeLaRiva, M. Wang, M.H. Engelhard, L. Kovarik, A.K. Datye, Y. Wang, Activation of surface lattice oxygen in single-atom Pt/CeO_2 for low-temperature CO oxidation, Science 358 (2017) 1419–1423. https://doi.org/10.1126/science.aao2109.
[31] J. Resasco, L. DeRita, S. Dai, J.P. Chada, M. Xu, X. Yan, J. Finzel, S. Hanukovich, A.S. Hoffman, G.W. Graham, S.R. Bare, X. Pan, P. Christopher, Uniformity Is Key in Defining Structure–Function Relationships for Atomically Dispersed Metal Catalysts: The Case of Pt/CeO_2, J. Am. Chem. Soc. 142 (2020) 169–184. https://doi.org/10.1021/jacs.9b09156.
[32] S. Loridant, Raman spectroscopy as a powerful tool to characterize ceria-based catalysts, Catal. Today 373 (2021) 98–111. https://doi.org/10.1016/j.cattod.2020.03.044.
[33] M.S. Brogan, T.J. Dines, J.A. Cairns, Raman spectroscopic study of the $Pt–CeO_2$ interaction in the $Pt/Al_2O_3–CeO_2$ catalyst, J. Chem. Soc. Faraday Trans. 90 (1994) 1461–1466. https://doi.org/10.1039/FT9949001461.
[34] G.W. Graham, W.H. Weber, J.R. McBride, C.R. Peters, Raman investigation of simple and complex oxides of platinum, J. Raman Spectrosc. 22 (1991) 1–9. https://doi.org/10.1002/jrs.1250220102.
[35] S. Chen, T. Cao, Y. Gao, D. Li, F. Xiong, W. Huang, Probing Surface Structures of CeO_2, TiO_2, and Cu_2O Nanocrystals with CO and CO_2 Chemisorption, J. Phys. Chem. C 120 (2016) 21472–21485. https://doi.org/10.1021/acs.jpcc.6b06158.
[36] G. Busca, Spectroscopic characterization of the acid properties of metal oxide catalysts, Catal. Today 41 (1998) 191–206. https://doi.org/10.1016/S0920-5861(98)00049-2.
[37] O. Pozdnyakova, D. Teschner, A. Wootsch, J. Kröhnert, B. Steinhauer, H. Sauer, L. Toth, F.C. Jentoft, A. Knop-Gericke, Z. Paál, R. Schlögl, Preferential CO oxidation in hydrogen (PROX) on ceria-supported catalysts, part I: Oxidation state and surface species on Pt/CeO_2 under reaction conditions, J. Catal. 237 (2006) 1–16. https://doi.org/10.1016/j.jcat.2005.10.014.
[38] C. Binet, M. Daturi, J.-C. Lavalley, IR study of polycrystalline ceria properties in oxidised and reduced states, Catal. Today 50 (1999) 207–225. https://doi.org/10.1016/S0920-5861(98)00504-5.
[39] J.C. Lavalley, Infrared spectrometric studies of the surface basicity of metal oxides and zeolites using adsorbed probe molecules, Catal. Today 27 (1996) 377–401. https://doi.org/10.1016/0920-5861(95)00161-1.
[40] W. Ruettinger, X. Liu, R.J. Farrauto, Mechanism of aging for a Pt/CeO_2-ZrO_2 water gas shift catalyst, Appl. Catal. B Environ. 65 (2006) 135–141. https://doi.org/10.1016/j.apcatb.2006.01.005.
[41] J.M. Zalc, V. Sokolovskii, D.G. Löffler, Are Noble Metal-Based Water–Gas Shift Catalysts Practical for Automotive Fuel Processing?, J. Catal. 206 (2002) 169–171. https://doi.org/10.1006/jcat.2001.3465.
[42] S. Hilaire, X. Wang, T. Luo, R.J. Gorte, J. Wagner, A comparative study of water-gas-shift reaction over ceria-supported metallic catalysts, Appl. Catal. Gen. 258 (2004) 271–276. https://doi.org/10.1016/j.apcata.2003.09.026.

[43] X. Liu, W. Ruettinger, X. Xu, R. Farrauto, Deactivation of Pt/CeO_2 water-gas shift catalysts due to shutdown/startup modes for fuel cell applications, Appl. Catal. B Environ. 56 (2005) 69–75. https://doi.org/10.1016/j.apcatb.2004.04.026.
[44] T. Jin, Y. Zhou, G.J. Mains, J.M. White, Infrared and x-ray photoelectron spectroscopy study of carbon monoxide and carbon dioxide on platinum/ceria, J. Phys. Chem. 91 (1987) 5931–5937. https://doi.org/10.1021/j100307a023.
[45] M. Di, K. Simmance, A. Schaefer, Y. Feng, F. Hemmingsson, M. Skoglundh, T. Bell, D. Thompsett, L.I. Ajakaiye Jensen, S. Blomberg, P.-A. Carlsson, Chasing PtO_x species in ceria supported platinum during CO oxidation extinction with correlative operando spectroscopic techniques, J. Catal. 409 (2022) 1–11. https://doi.org/10.1016/j.jcat.2022.03.022.
[46] T.Y. Kardash, E.A. Derevyannikova, E.M. Slavinskaya, A.I. Stadnichenko, V.A. Maltsev, A.V. Zaikovskii, S.A. Novopashin, A.I. Boronin, K.M. Neyman, Pt/CeO_2 and $Pt/CeSnO_x$ Catalysts for Low-Temperature CO Oxidation Prepared by Plasma-Arc Technique, Front. Chem. 7 (2019). https://www.frontiersin.org/articles/10.3389/fchem.2019.00114 (accessed July 24, 2023).
[47] A.I. Boronin, E.M. Slavinskaya, A. Figueroba, A.I. Stadnichenko, T.Yu. Kardash, O.A. Stonkus, E.A. Fedorova, V.V. Muravev, V.A. Svetlichnyi, A. Bruix, K.M. Neyman, CO oxidation activity of Pt/CeO2 catalysts below 0 °C: platinum loading effects, Appl. Catal. B Environ. 286 (2021) 119931. https://doi.org/10.1016/j.apcatb.2021.119931.
[48] A. Martínez-Arias, D. Gamarra, M. Fernández-García, A. Hornés, P. Bera, Zs. Koppány, Z. Schay, Redox-catalytic correlations in oxidised copper-ceria CO-PROX catalysts, Catal. Today 143 (2009) 211–217. https://doi.org/10.1016/j.cattod.2008.09.018.
[49] H. Zhu, Z. Qin, W. Shan, W. Shen, J. Wang, Pd/CeO2–TiO2 catalyst for CO oxidation at low temperature: a TPR study with H_2 and CO as reducing agents, J. Catal. 225 (2004) 267–277. https://doi.org/10.1016/j.jcat.2004.04.006.
[50] C. Serre, F. Garin, G. Belot, G. Maire, Reactivity of Pt/Al_2O_3 and $Pt\text{-}CeO_2Al_2O_3$ Catalysts for the Oxidation of Carbon Monoxide by Oxygen: II. Influence of the Pretreatment Step on the Oxidation Mechanism, J. Catal. 141 (1993) 9–20. https://doi.org/10.1006/jcat.1993.1114.
[51] A. Martínez-Arias, R. Cataluña, J.C. Conesa, J. Soria, Effect of Copper−Ceria Interactions on Copper Reduction in a $Cu/CeO_2/Al_2O_3$ Catalyst Subjected to Thermal Treatments in CO, J. Phys. Chem. B 102 (1998) 809–817. https://doi.org/10.1021/jp972097q.
[52] S. Ricote, G. Jacobs, M. Milling, Y. Ji, P.M. Patterson, B.H. Davis, Low temperature water–gas shift: Characterization and testing of binary mixed oxides of ceria and zirconia promoted with Pt, Appl. Catal. Gen. 303 (2006) 35–47. https://doi.org/10.1016/j.apcata.2006.01.025.
[53] P. Bazin, O. Saur, J.C. Lavalley, M. Daturi, G. Blanchard, FT-IR study of CO adsorption on Pt/CeO_2: characterisation and structural rearrangement of small Pt particles, Phys. Chem. Chem. Phys. 7 (2005) 187–194. https://doi.org/10.1039/B414159H.
[54] P. Panagiotopoulou, D.I. Kondarides, A comparative study of the water-gas shift activity of Pt catalysts supported on single (MO_x) and composite (MO_x/Al_2O_3, MO_x/TiO_2) metal oxide carriers, Catal. Today 127 (2007) 319–329. https://doi.org/10.1016/j.cattod.2007.05.010.
[55] G. Busca, J. Lamotte, J.C. Lavalley, V. Lorenzelli, FT-IR study of the adsorption and transformation of formaldehyde on oxide surfaces, J. Am. Chem. Soc. 109 (1987) 5197–5202. https://doi.org/10.1021/ja00251a025.

[56] A. Badri, C. Binet, J.-C. Lavalley, An FTIR study of surface ceria hydroxy groups during a redox process with H_2, J. Chem. Soc. Faraday Trans. 92 (1996) 4669–4673. https://doi.org/10.1039/FT9969204669.
[57] A. Laachir, V. Perrichon, A. Badri, J. Lamotte, E. Catherine, J.C. Lavalley, J.E. Fallah, L. Hilaire, F.L. Normand, E. Quéméré, G.N. Sauvion, O. Touret, Reduction of CeO_2 by hydrogen. Magnetic susceptibility and Fourier-transform infrared, ultraviolet and X-ray photoelectron spectroscopy measurements, J. Chem. Soc. Faraday Trans. 87 (1991) 1601–1609. https://doi.org/10.1039/FT9918701601.
[58] C. Binet, A. Badri, J.-C. Lavalley, A Spectroscopic Characterization of the Reduction of Ceria from Electronic Transitions of Intrinsic Point Defects, J. Phys. Chem. 98 (1994) 6392–6398. https://doi.org/10.1021/j100076a025.
[59] Ch. Vignatti, M.S. Avila, C.R. Apesteguía, T.F. Garetto, Catalytic and DRIFTS study of the WGS reaction on Pt-based catalysts, Int. J. Hydrog. Energy 35 (2010) 7302–7312. https://doi.org/10.1016/j.ijhydene.2010.04.180.
[60] A. Holmgren, B. Andersson, D. Duprez, Interactions of CO with Pt/ceria catalysts, Appl. Catal. B Environ. 22 (1999) 215–230. https://doi.org/10.1016/S0926-3373(99)00047-8.
[61] C. Li, Y. Sakata, T. Arai, K. Domen, K. Maruya, T. Onishi, Adsorption of carbon monoxide and carbon dioxide on cerium oxide studied by Fourier-transform infrared spectroscopy. Part 2.—Formation of formate species on partially reduced CeO_2 at room temperature, J. Chem. Soc. Faraday Trans. 1 Phys. Chem. Condens. Phases 85 (1989) 1451–1461. https://doi.org/10.1039/F19898501451.
[62] K. Yoshikawa, H. Sato, M. Kaneeda, J.N. Kondo, Synthesis and analysis of CO2 adsorbents based on cerium oxide, J. CO_2 Util. 8 (2014) 34–38. https://doi.org/10.1016/j.jcou.2014.10.001.
[63] T. Shido, Y. Iwasawa, Regulation of reaction intermediate by reactant in the water-gas shift reaction on CeO_2, in relation to reactant-promoted mechanism, J. Catal. 136 (1992) 493–503. https://doi.org/10.1016/0021-9517(92)90079-W.
[64] R. Jain, A.S. Poyraz, D.P. Gamliel, J. Valla, S.L. Suib, R. Maric, Comparative study for low temperature water-gas shift reaction on Pt/ceria catalysts: Role of different ceria supports, Appl. Catal. Gen. 507 (2015) 1–13. https://doi.org/10.1016/j.apcata.2015.09.041.
[65] A.M. Gänzler, M. Casapu, P. Vernoux, S. Loridant, F.J. Cadete Santos Aires, T. Epicier, B. Betz, R. Hoyer, J.-D. Grunwaldt, Tuning the Structure of Platinum Particles on Ceria In Situ for Enhancing the Catalytic Performance of Exhaust Gas Catalysts, Angew. Chem. Int. Ed. 56 (2017) 13078–13082. https://doi.org/10.1002/anie.201707842.
[66] X. Li, X. Wang, I.I. Sadykov, D. Palagin, O.V. Safonova, J. Li, A. Beck, F. Krumeich, J.A. van Bokhoven, L. Artiglia, Temperature and Reaction Environment Influence the Nature of Platinum Species Supported on Ceria, ACS Catal. 11 (2021) 13041–13049. https://doi.org/10.1021/acscatal.1c03165.
[67] H. Frey, A. Beck, X. Huang, J.A. van Bokhoven, M.G. Willinger, Dynamic interplay between metal nanoparticles and oxide support under redox conditions, Science 376 (2022) 982–987. https://doi.org/10.1126/science.abm3371.
[68] L. Piccolo, S. Loridant, P. Christopher, Supported Metal Single-Atom Thermocatalysts for Oxidation Reactions, in: Support. Met. Single At. Catal., John Wiley & Sons, Ltd, 2022: pp. 377–423. https://doi.org/10.1002/9783527830169.ch9.
[69] S. Xie, L. Liu, Y. Lu, C. Wang, S. Cao, W. Diao, J. Deng, W. Tan, L. Ma, S.N. Ehrlich, Y. Li, Y. Zhang, K. Ye, H. Xin, M. Flytzani-Stephanopoulos, F. Liu, Pt Atomic Single-Layer

Catalyst Embedded in Defect-Enriched Ceria for Efficient CO Oxidation, J. Am. Chem. Soc. 144 (2022) 21255–21266. https://doi.org/10.1021/jacs.2c08902.
[70] J. Lee, Y. Ryou, J. Kim, X. Chan, T.J. Kim, D.H. Kim, Influence of the Defect Concentration of Ceria on the Pt Dispersion and the CO Oxidation Activity of Pt/CeO_2, J. Phys. Chem. C 122 (2018) 4972–4983. https://doi.org/10.1021/acs.jpcc.8b00254.
[71] X.I. Pereira-Hernández, A. DeLaRiva, V. Muravev, D. Kunwar, H. Xiong, B. Sudduth, M. Engelhard, L. Kovarik, E.J.M. Hensen, Y. Wang, A.K. Datye, Tuning $Pt\text{-}CeO_2$ interactions by high-temperature vapor-phase synthesis for improved reducibility of lattice oxygen, Nat. Commun. 10 (2019) 1358. https://doi.org/10.1038/s41467-019-09308-5.
[72] C. Molinet-Chinaglia, L. Piccolo, S. Loridant, Investigating the Dynamics of Pt/CeO_2 Catalysts at the Powder Agglomerate Scale by Combining In Situ Hyperspectral Raman Imaging and SEM-EDX Analysis, ChemCatChem 15 (2023) e202300627. https://doi.org/10.1002/cctc.202300627.